

IMPACT BEHAVIOUR OF HYBRID TIMBER BEAMS

Bryan E. Thevarajah¹, Alex M. Remennikov², Tuan D. Ngo³, Hong Guan⁴, Benoit P. Gilbert⁵

ABSTRACT: Recent technological developments in the manufacturing of engineered wood products (EWP) have positioned mass solid timber (MST) systems as front-runners as a viable alternative construction material due to their lightweight character and low carbon footprint. Key limitations associated with the MST systems are their brittle behaviour and low stiffness. These limitations are exacerbated in the event of a critical structural member's failure due to deliberate or accidental extreme loads, such as impacts and blasts, which could lead to the progressive collapse of a building. This study aims to investigate the performance of timber beams specifically laminated veneer lumber (LVL) and the effects of hybridizing timber beams with fibre-reinforced polymer (FRP) and steel as a solution to overcome these shortcomings. A series of control and hybrid beams, fabricated with commercially available LVL, were studied under quasi-static and impact loading conditions. The LVL beams were strengthened with surface-mounted carbon fibre-reinforced polymer (CFRP) sheets, near-surface mounted glass fibre-reinforced polymer (GFRP) rods, screwed-in steel plates and glue-mounted steel plates. Dynamic impact loads were simulated using a free-falling drop hammer test setup, with a high-speed data acquisition system recording the impact loads and associated displacements. Additionally, a high-speed 3D Digital Image Correlation (DIC) system was employed to capture a comprehensive three-dimensional strain field and inspect the modes of failure. The effects of various hybridization techniques and materials on the behaviour and performance of the timber beams are discussed in detail.

KEYWORDS: laminated veneer lumber, hybrid timber beams, impact, ductility, digital image correlation

1 – INTRODUCTION

Global urbanization along with rapidly growing population have raised the demand for new dwellings. The extensive use of high carbon footprint materials such as concrete and steel, coupled with increasing demand, poses significant environmental challenges, given construction industry accounted for approximately 39% of the global greenhouse gas emissions [1]. Engineered wood products (EWP) specifically mass solid timber (MST) systems are regaining popularity with

advancements in manufacturing technologies due to the low carbon footprint nature and high potential for recycling compared to the conventional construction materials [2-4]. The potential to utilize EWP systems in construction has greatly increased with the 2019 National Construction Code of Australia allowing timber buildings up to 25 metres for all building classes, subject to the Deemed-to-Satisfy requirements [5]. Cross-laminated timber (CLT), laminated veneer lumber (LVL), and glulam are some of the widely used MST systems. Since EWP systems are made of natural wood,

¹ Bryan Eric Thevarajah, School of Civil, Mining, Environmental, and Architectural Engineering, The University of Wollongong, Wollongong, Australia, tbryan@uow.edu.au

² Alex M. Remennikov, School of Civil, Mining, Environmental, and Architectural Engineering, The University of Wollongong, Wollongong, Australia, alexrem@uow.edu.au

³ Tuan D. Ngo, Department of Infrastructure Engineering, The University of Melbourne, Parkville, Australia, dtngo@unimelb.edu.au

⁴ Hong Guan, School of Engineering and Built Environment, Griffith University, Gold Coast, Australia, h.guan@griffith.edu.au

⁵ Benoit Gilbert, School of Engineering and Built Environment, Griffith University, Gold Coast, Australia, b.gilbert@griffith.edu.au

the inherent brittle nature of wood results in lack of robustness and structural resilience of MST systems. This vulnerability has been highlighted by instances of timber structure collapses reported in Germany, Denmark, and Finland. Investigations into these failures have identified key contributing factors, including the inherently brittle behaviour and relatively low stiffness of EWP structural members, as well as the limited ductility of their connections, which can trigger progressive collapse mechanisms [6, 7]. This underlying shortcoming can be amplified in an event of extreme loads such as impacts and blasts. As timber systems are adapted in taller buildings, it is crucial to consider their structural resilience.

Hybrid timber systems have been extensively studied to mitigate the aforementioned limitations by combining various materials with timber with enhanced the overall performance and structural resilience [8-18]. Combining MST with high-strength materials, such as steel or fibre reinforced polymers (FRPs) can create robust hybrid timber systems with improved ductility and energy absorption while taking advantage of the lightweight and low carbon footprint nature of timber. While widespread research exists on hybrid timber systems under static and cyclic loads, there is limited knowledge on their performance under extreme loads. Early studies in the impact behaviour of timber focused widely on clear wood specimens and some studies investigating the effect of natural defects such as knots [19-21]. While most studies have reported increase in dynamic strength, there are instances of contradicting observations of reduced dynamic strengths due to the quality of the specimen [19, 21-25]. Localised crushing of wood fibres at the impact zone was reported on a dynamic impact study on parallel strand lumber [26]. Recent studies on high strain rates effects simulated by shock tube on wide range of mass timber systems such as glulam, CLT and light-frame wood stud walls have guided in formulating blast design guidelines and considerations [27-31]. While extensive work has been done on CLT and glulam, limited work has been done on the behaviour of LVL and the effects of dynamic impact loads on hybrid timber beams. This series of experimental study focuses on the flexural response of hybrid timber, specifically LVL beams under quasi-static and dynamic impact loading conditions.

2 – EXPERIMENTAL PROGRAMME

2.1 Materials and specimens' construction

A total of 7 beams were tested under static loading conditions and 7 beams were tested under dynamic

impact loading conditions. LVL beams specimens were sourced from commercially available wesbeam e-beam E13 LVL with a cross-section of 150 × 63 mm. The LVL beams were cut to 2100 mm lengths from delivered lengths of 6.3 m beams. Various hybridization techniques were applied on the acquired lengths of beams to compare the performance and improvements in stiffness, peak capacity, ductility. Fig. 1 shows the cross-sections of the beams investigated under this experimental programme and the Table 1 presents the summary of the static and impact test specimens.

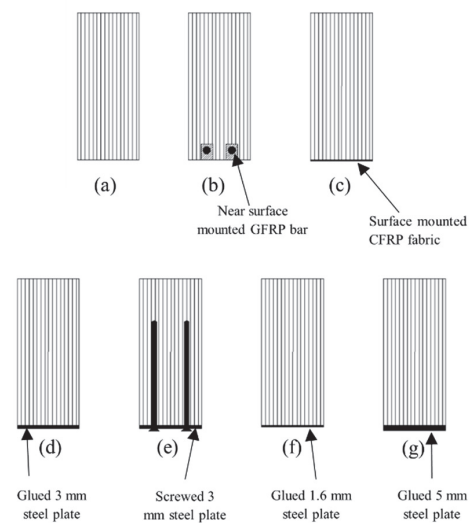


Figure 1. Beam specimen cross-sections

A layer of unidirectional carbon fibre reinforced polymer (CFRP) fabric was surface mounted on the tension face of the beams for type 2 beams. Two grooves were cut using wood routers to near surface mount 2 numbers of 8 mm diameter glass fibre reinforced polymer (GFRP) rods on the tension side for type 3 beams. For type 4 and 5 beams, 3 mm thick steel plate with a width of 50 mm was surface mounted using self-tapping structural timber screws and bonded with polyurethane (PUR) structural adhesive respectively.

Table 1. Summary of beam specimens

No.	Specimen		Beam type
	Static	Dynamic	
(a)	S-01	D-01	Control
(b)	RS-01	RD-01	NSM 10 mm GFRP rods
(c)	RS-02	RD-02	SM CFRP fabric
(d)	RS-03	RD-03	Glued 3 mm steel
(e)	RS-04	RD-04	Screwed 3mm steel
(f)	RS-05	RD-05	Glued 1.6 mm steel
(g)	RS-06	RD-06	Glued 5 mm steel

2.2 Static test setup

The static beams were simply supported and subjected to a three-point bending configuration, to simulate a localised impact event rather than a constant moment region which is unlikely during an impact. The clear span length was 2000 mm, with 50 mm overhang on the sides. Quasi-static loads were applied using a hydraulic actuator equipped with a 900 kN load cell at a displacement rate of 5 mm/min. The quasi-static test configuration is shown in Fig. 2. While the load cell measured the force that the beams sustained, three methods of displacement measurements were utilised during the static tests; laser displacement sensor positioned under the midspan of the beam, linear variable displacement transducers (LVDT) in the hydraulic actuators, and a 3D digital image correlation (DIC) system. The employment of 3D DIC system allowed for continuous full-field strain measurements and inspection of failure modes in post processing. The data acquisition was conducted at a rate of 1 sample per second.

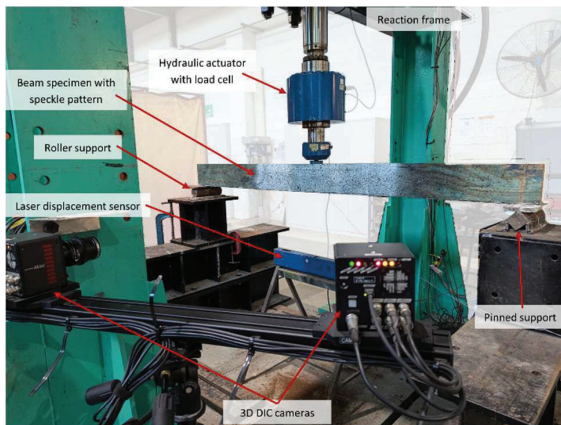


Figure 2. Static experimental setup

2.3 Dynamic test setup

The dynamic experimental setup procedure started with the positioning of two sturdy steel supports on a strong floor to allow the timber beams to have a clear span of 2000 mm and an overhang of 50 mm on each side. All beams were tested under three-point loading and simply supported on steel rollers to closely replicate the conditions of the static test setup. The beam specimens were secured with a bracket to prevent any rebounds of the beams while ensuring no additional resistance was provided from the brackets to the applied loads. The dynamic impact loads were generated by a drop hammer facility. The drop hammer assembly is attached to a guide rail with low-friction rollers to minimise any losses and

simulate free-fall. The drop hammer assembly is raised and held at desired height with an electric powered motor with integrated clutch. The impact energy can be varied by changing the weight and/or height of the drop hammer. Although the weight of the drop hammer can be changed by adding or removing lead pellets, for this experimental programme, the weight of the drop hammer was kept at 100 kg which included the impact tup and a dynamic load cell assembly and different heights were selected to simulate various impact energies. The drop hammer was released by pulling a cord attached to a trigger mechanism which allows to drop hammer to free-fall. The dynamic impact loads and support reactions were recorded by the dynamic load cells located in the drop hammer assembly and the supports respectively through a high-speed data acquisition (DAQ) system at a rate of 10,000 samples per second. The resulting displacements and the full-field strain measurements were captured by a high-speed 3D DIC system at 3000 frames per second. Both high-speed DAQ and the 3D DIC system was trigger synced by a 5V voltage signal which was triggered with a push button simultaneously when the drop hammer is released. The high-speed image series obtained from the 3D DIC system were post-processed in GOM Correlate Pro to obtain displacements and strain measurements and inspection of failure modes. Fig. 3 illustrates the experimental setup.

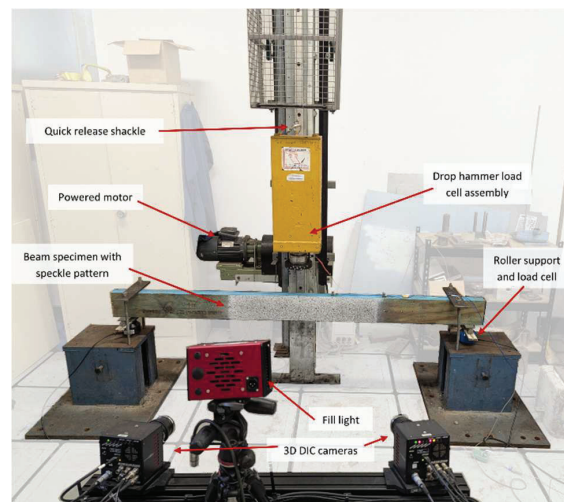


Figure 3. Dynamic impact testing setup

3 – RESULTS AND DISCUSSION

3.1 Static test

Under quasi-static loading, control beam specimen S-01 exhibited tensile failure without any signs of crushing in the compression zone until failure, as shown in Fig. 4a.

The hybridisation of the timber beams resulted in variations in failure modes and significant improvements in post-peak behaviour. Compression crushing in timber (Fig. 4b) prior to the peak was observed in hybrid beams RS-01, RS-02, RS-03, and RS-06. While RS-01, RS-02, and RS-03 failed in tension following compression crushing at peak load, RS-06 exhibited shear failure as shown in Fig. 4c. Post-peak compression crushing of timber was evident in beams RS-01, RS-02, RS-03, and RS-06, with RS-03 also demonstrating significant steel yielding. In contrast, beam specimens RS-04 and RS-05 did not exhibit compression crushing before reaching peak load, similar to the control beams. However, in the post-peak stage, both steel yielding and compression crushing were recorded in RS-04 and RS-05.

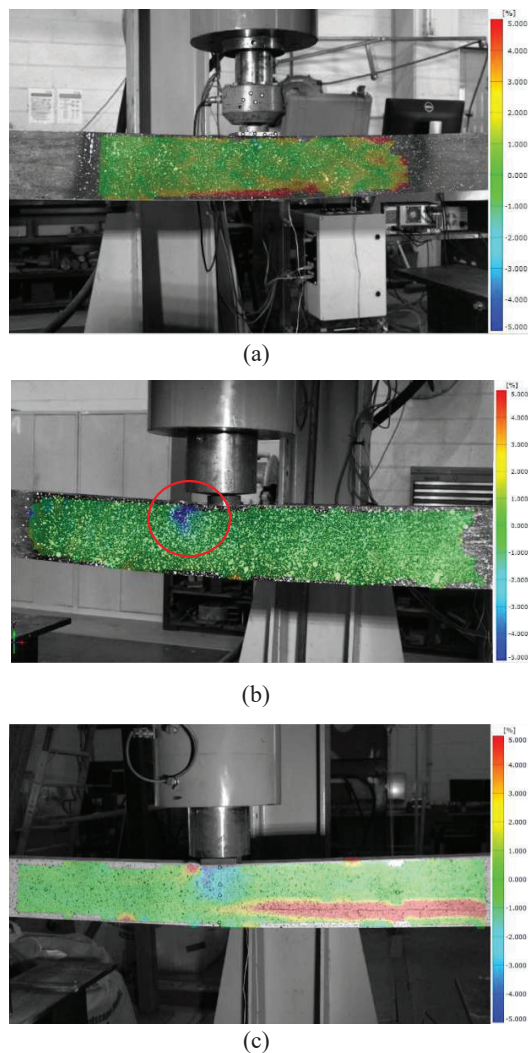


Figure 4. Strain fields at (a) tensile failure; (b) compression crushing; (c) shear failure of timber during quasi-static tests

The load-deflection behaviour of the beams under quasi-static loading is presented in Fig. 5. The summary of the experimental results including stiffness (K), ultimate load (P_u), ultimate moment capacity (M_u), deflection at the elastic limit (Δ_e), total deflection (Δ_m), and ductility ratio (μ), are summarised in Table 2. The ductility ratio is the ratio between total and elastic limit deflections as shown in (1). Stiffness was determined by linear regression within a region of 10 to 40 per cent of the ultimate load [32, 33]. The proportional limit where the load-deflection behaviour deviates from linearity was assumed to be the elastic limit, and the total deflection was assumed to be the greatest of the deflection at the ultimate load or 80% of the ultimate load [34-37].

$$\mu = \Delta_m / \Delta_e \quad (1)$$

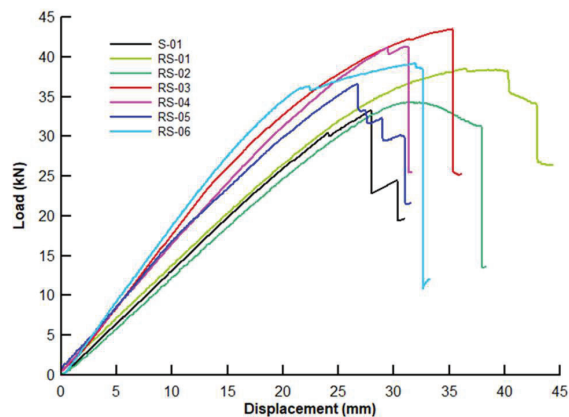


Figure 5. Load-displacement plots for static tests

Table 2. Summary of Static test results

Beam	K (kN/m)	P_u (kN)	M_u (kNm)	Δ_e (mm)	Δ_m (mm)	μ
S-01	1320.2	33.4	18.1	20.8	27.9	1.34
RS-01	1322.3	38.5	16.7	20.8	42.8	2.06
RS-02	1260.5	34.3	15.9	22.7	37.8	1.67
RS-03	1762.3	43.5	19.2	14.2	35.2	2.48
RS-04	1645.1	41.3	17.2	19.0	31.3	1.64
RS-05	1645.1	36.6	21.7	13.3	30.9	2.32
RS-06	1860.5	39.2	20.7	16.2	32.6	2.01

Under the static loading, all beams exhibited an initial linear elastic response. The beams with FRP reinforcements (RS-01, RS-02) exhibited similar stiffnesses compared to the control beam while the hybrid timber-steel beams (RS-03 – RS-06) showed a significant increase with RS-06 recording almost 41% rise. Surprisingly, RS-02 which was strengthened with

surface-mounted CFRP demonstrated the lowest stiffness. This could have been a result of a weakness in the specific timber specimen as any other plausible explanation could not be attributed to this.

The peak load and the moment capacity of all the hybrid beams showed improvement with the highest enhancement of about 30% in RS-03. RS-04, RS-06 and RS-01 also recorded notable increases around 24%, 17%, and 15% respectively. The onset of shear failure in RS-06 could have been attributed to this reduction. RS-02 and RS-05 showed only moderate gains, ranging from 2% to 10%, suggesting less effectiveness under static loading.

Similar to the previous observations, hybridization significantly improved the ductility ratios compared to the control beam, with RS-03 and RS-05 showing the highest enhancements around 85% and 73% increase. RS-01 and RS-06 also demonstrated notable improvements to reach a ductility ratio of 2, approximately a 50% rise in ductility while RS-02 and RS-04 showed only moderate gains around 23%. It is evident that when the thickness of the steel plate is increased, ductility seems to reduce due to the onset of shear failure.

3.2 Dynamic impact tests

The midspan displacement-time histories of beams subjected to an impact velocity of 3.4 m/s and a corresponding impact energy of 589 J are presented in Fig. 6. Hybridization with steel plates significantly improved deflection control, particularly in beams with glue-mounted steel plates. Beams RD-03 and RD-06, reinforced with 3 mm and 5 mm steel plates, showed a 32% and 30% reduction in peak deflection, respectively, compared to the control beam. Beams hybridized with surface-mounted CFRP, and a glue-mounted 0.8 mm steel plate demonstrated comparable performance, each achieving a 22% reduction. The screw-mounted 3 mm steel plate (RD-04) showed intermediate performance, with a 27% reduction in deflection. The lowest reduction in deflection (13%) was observed in RD-01, which may be attributed to a loss of stiffness due to the grooves cut in the timber to accommodate the NSM GFRP bars. Furthermore, it should be noted that the control beam D-01 failed under the applied impact load, whereas none of the hybrid beams exhibited any damages under the full-field strain inspection.

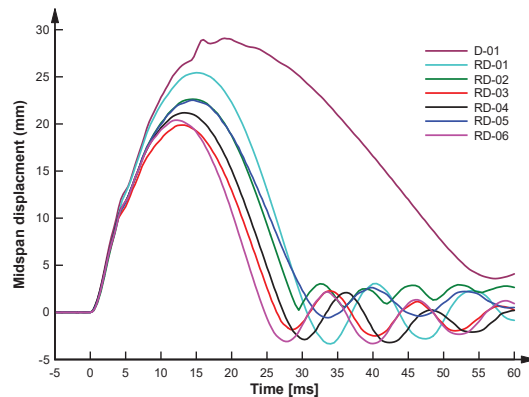


Figure 6. Displacement time histories under 3.4 m/s impact

The dynamic impact loading shifted failure modes in some beam specimens and did not influence in others. Under dynamic impact loading, the control beam D-01 and hybrid beams RD-02, RD-03, and RD-05 exhibited failure modes and progression similar to their static counterparts. The control beam D-01 failed due to tensile rupture of timber without any signs of compression crushing, consistent with its behaviour under static loading. The CFRP surface-mounted hybrid beam RD-02 failed in tension with compression crushing of timber. However, when subjected to a subsequent impact drop, the beam collapsed, accompanied by CFRP fabric delamination which was not observed in static testing, indicating a progressive failure mechanism under repeated loading. The beams hybridised with glued steel plates (RD-03 and RD-06, reinforced with 3 mm and 5 mm steel plates, respectively) exhibited compression crushing followed by tensile failure of timber under dynamic loading, whereas under static loading, RS-06 failed in shear following compression crushing. Compared to their static counterparts, RD-03 and RD-06 exhibited more extensive bearing damage in the impact zone, indicating localised energy absorption by timber. Both RD-04 and RD-05 failed by tensile rupture of timber, consistent with their failure modes under static loading. However, RD-04 exhibited additional shear failure of timber just above the inclined screws, which was not observed under static loading, suggesting that the fasteners influenced shear stress distribution under impact conditions. A notable deviation was observed in RD-01, which was hybridised with NSM-mounted GFRP rods. Under dynamic loading, RD-01 failed in shear, whereas its static counterpart failed through compression crushing followed by tensile failure. This variation indicates that the strain rate effects under impact conditions may have altered the failure mechanism, leading to an earlier shear failure.

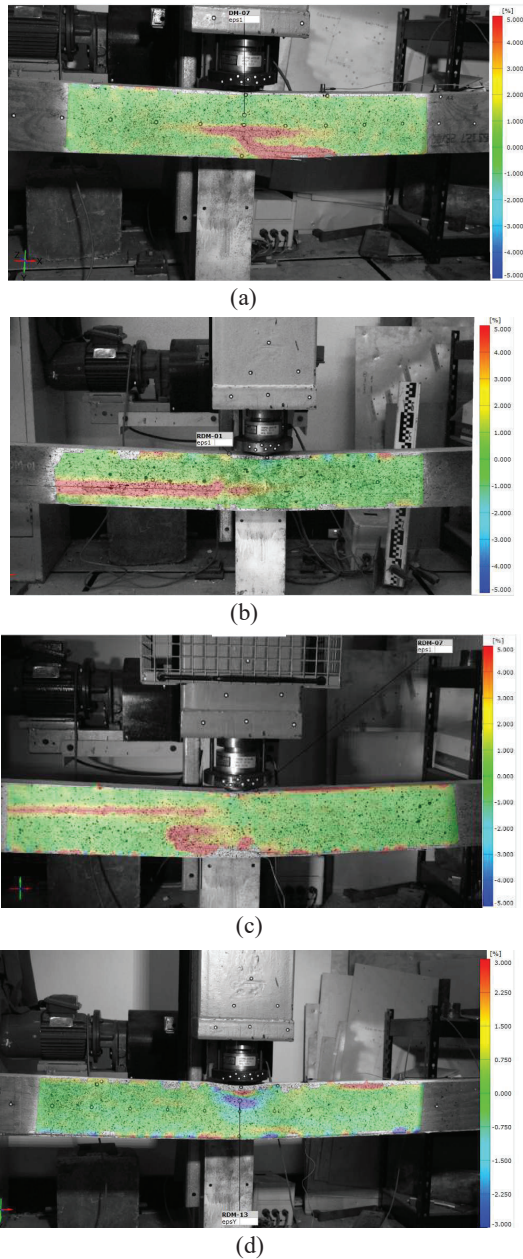


Figure 7. Strain fields at (a) tensile failure; (b) shear failure; (c) combination of shear and tensile failure; (d) compression crushing of timber during dynamic tests

As the impact energies were higher for hybrid beams, localised fibre crushing and laminate splitting were observed in all specimens as displayed in Fig. 8. Further investigations are ongoing to determine and quantify energy dissipation from localised fibre crushing.

When subjected to an impact load from a falling mass, the impact force is resisted by a transient mechanism of

inertial and flexural resistance. Initially, when the drop hammer contacts the beam, the beam accelerates in the direction of the applied impact force generating inertial forces in the opposite direction. A brief separation was observed between the beam and the drop hammer as the beam accelerates away from the drop hammer and a drop in impact force was recorded. The drop hammer then catches up with the beam to apply the rest of the impact force. The vertical equilibrium of the beam specimen subjected to a dynamic impact force from a falling mass as a function of time is given in (2).

$$\int_0^L \bar{m}a(x, t) dx + R_1(t) + R_2(t) = I(t) \quad (2)$$

where L is the length of the beam, \bar{m} is the mass per unit length of the beam, a is the acceleration at a given point along the beam, R_1, R_2 are the support reactions, and I is the impact force. The term $\int_0^L \bar{m}a(x, t) dx$ indicates the inertial resistance. Impact force, total reaction forces and inertial force time histories for a period of 40 ms from the initial impact are presented in Fig. 9 for control beam D-01 from a drop height of 500 mm.

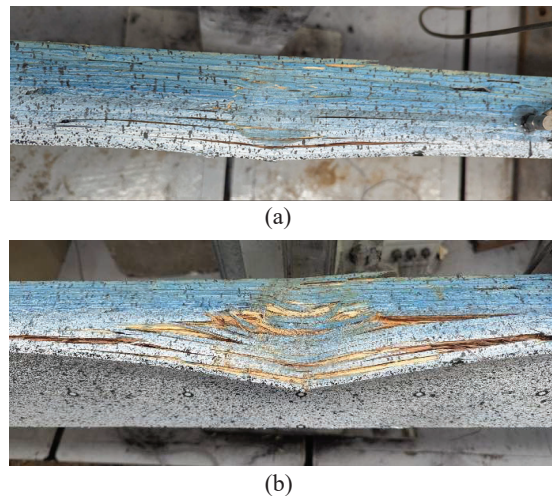


Figure 8. Localised fibre crushing and laminate splitting (a) after first drop from 600 mm; (b) after subsequent drop from 1600 mm

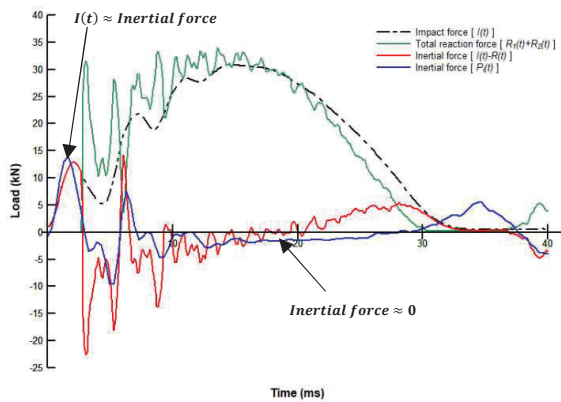


Figure 9. Force history of a dynamic impact test

Initially, the impact forces are resisted by inertial forces for about 2.5 ms from initial impact during which the reaction load cells did not register any forces as shown in the force history. Once the stress waves reach the supports, the applied force is resisted by both inertial resistance and flexural resistance. Around $t=17.3$ ms when the impact force reaches the peak, the inertial force averages near zero at which point the impact forces are mostly resisted by flexural resistance. Inertial force (P_i) is calculated using (3) which assumes a sinusoidal acceleration distribution consistent with the deflected shape of the beam in the elastic range, as suggested by previous studies [19, 26, 38-40]. The resulting inertial force history aligns well with the measured inertial response $I(t) - [R_1(t) + R_2(t)]$ as demonstrated in Fig. 9, during the initial stage of impact (up to approximately 2.5 ms from the initial contact). Within this period, the acceleration across the beam closely follows a sinusoidal distribution as shown in Fig 9(a). However, as the beam begins to vibrate in higher modes, the acceleration profile across the beam deviates from the assumed sinusoidal profile as illustrated in Fig. 10 (b), (c), and (d), resulting the estimations from (1) less accurate over the time.

$$P_i(t) = \bar{m}a_0(t) \left[\frac{l}{2} + \frac{2\pi^2(h)^3}{3l^2} \right] \quad (3)$$

where l is the clear span of the beam, $a_0(t)$ is the acceleration at the midspan of the beam, and h is the overhang length of the beam.

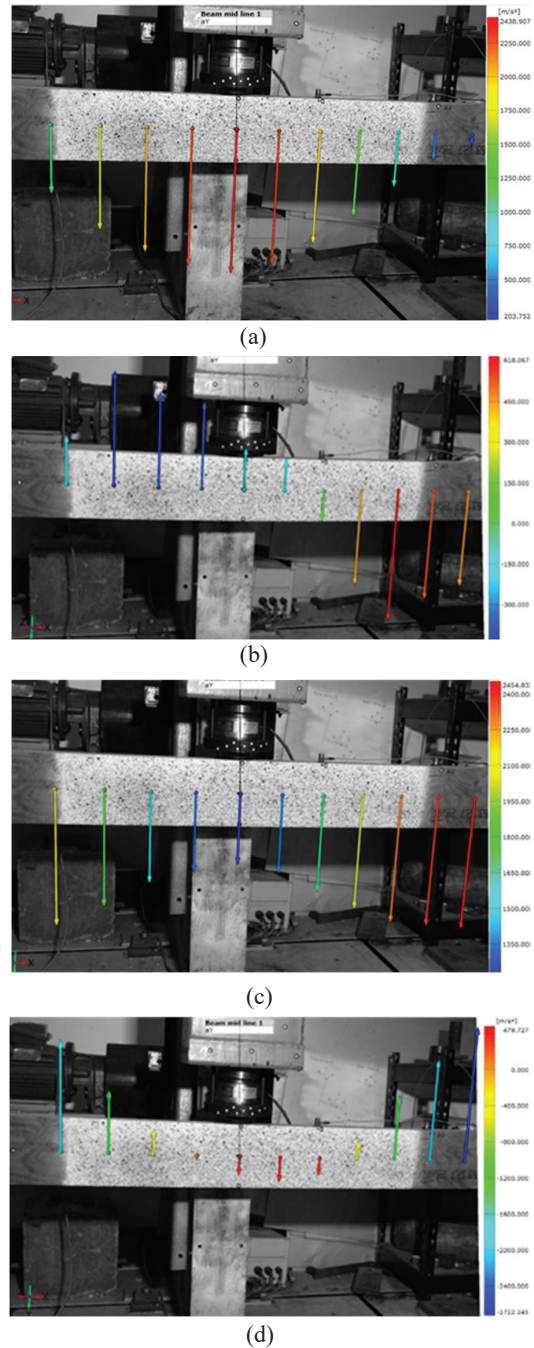


Figure 10. Acceleration distributions observed during impact (a) 1st mode; (b) 2nd mode; (c) and (d) 3rd mode

Although dynamic amplification due to impact loads are observed as illustrated in Fig. 9 which can affect the determination of the dynamic capacity of the beams, for comparison of the performance of the beam specimens, reactions were assumed to be half of the impact force, i.e. $R_1 = R_2 = I(t)/2$ simplifying the estimation of the

experimental dynamic moment capacities. The summary of impact energies (E_D) peak impact loads (P_{wi}), dynamic moment capacities (M_{wi}) and corresponding deflections at peak impact load (Δ_P) are presented in Table 3. The displacement-time histories for the drops corresponding to the failure of each beam is given in Fig. 11.

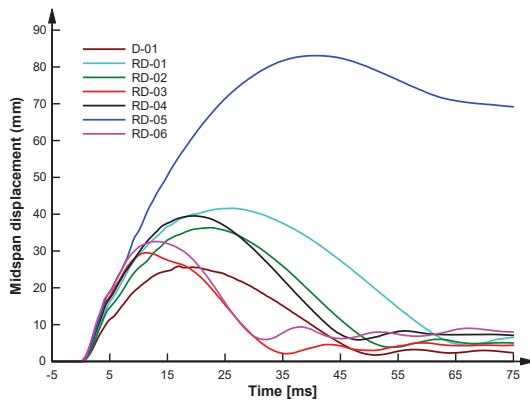


Figure 11. Displacement-time histories

Table 3. Summary of dynamic impact testing

Specimen	E_D (J)	P_{wi} (kN)	M_{wi} (kNm)	Δ_P (mm)
D-01	441	27.5	13.77	25.2
RD-01	981	35.9	17.95	32.3
RD-02	883	34.1	17.05	24.2
RD-03	1275	38.4	19.21	29.5
RD-04	1275	33.7	16.87	28.1
RD-05	1570	34.9	17.47	26.9
RD-06	1570	47.0	23.50	27.7

Compared to the control beam, all hybrid beams exhibited increased moment capacities under dynamic impact loading, with the most substantial improvements observed in beams with glued steel plates (RD-03, RD-05, RD-06) and the beam with near-surface mounted GFRP rods (RD-01). Notably, RD-06 which was hybridized with a glued 5 mm steel plate, demonstrated approximately a 58% increase in moment capacity relative to the control beam. When comparing the effect of mounting techniques, the beam hybridized with a glued steel plate (RD-03) outperformed the beam hybridized with a screw-mounted steel plate (RD-04). The glued hybrid beam resulted in higher moment capacity and delayed onset of tensile failure of timber, suggesting a more effective composite action between the timber and the steel. A general trend of increasing moment capacities with increasing steel thickness was observed. When the thickness of the steel plate was doubled from 1.6 mm to 3 mm, the moment capacity was

increased by 10%. When the plate thickness was nearly tripled to 5 mm, a 35% increase was recorded. In addition, increasing the plate thickness from 3 mm to 5 mm led to a 22% increase in moment capacity.

All hybrid beam configurations except RD-02 exhibited increased displacement at peak load compared to the control beam indicating enhanced ductility. Among these RD-01 showed the highest deformation increase of 28% compared to the control beam. Beams hybridized with 3 mm recorded a 17% and 11.5% increase in displacement for glued (RD-03) and screwed (RD-04) configurations respectively, suggesting the high effectiveness of the glue-mounting technique. Beams RD-06 and RD-05 which were strengthened with 5 mm and 1.6 mm steel plates respectively demonstrated a 10% and 6.7% increase in displacement compared to the control beam. In contrast, RD-02 which was strengthened with surface-mounted CFRP fabric, recorded a reduction of 4% compared to the control beam, indicating a stiffer and brittle behaviour.

4 – CONCLUSION

An experimental programme with fourteen LVL beams under static and dynamic impact loading has been presented and discussed the performance and effects of various hybridizing materials and techniques. The observations and experimental data analyses have led to the following key findings:

1. Hybridization of timber beams significantly enhanced performance in terms of stiffness, moment capacity and ductility under static and dynamic impact loading conditions.
2. FRP-based reinforcements including near-surface mounted GFRP rods and surface-mounted CFRP fabrics improved the overall performance under static and impact loadings. However, delamination and adhesive failure remain a critical concern under the high strain rate impact loading.
3. A shift in failure modes was observed in heavily reinforced beams transitioning between tensile failure and shear failure of timber, prompting the need for further investigation.
4. Glued steel reinforcement provides a better composite action between the timber and steel compared to a screw-mounted system, resulting in improved performance under both static and impact loading regimes.
5. Increasing steel plate thickness in hybrid timber-steel beams led to increased moment

capacity, though this came at the expense of reduced ductility, highlighting the need to balance strength and ductility during design.

- Higher modes of vibration were observed during dynamic impact loading, highlighting the need for a more accurate estimation of inertial loads.

ACKNOWLEDGEMENTS

The authors acknowledge the support given by technical officers Mr. Travis Marshall and Mr. Duncan Best of the University of Wollongong for their assistance with manufacturing specimens and conducting tests. This research was supported and funded by the Australian Research Council (ARC) under the Discovery Project DP210102499.

REFERENCES

- Global Alliance for Buildings and Construction, International Energy Agency and the United Nations Environment Programme, *2019 Global Status Report for Buildings and Construction: Towards a zero-emission, efficient and resilient buildings and construction sector*. 2019.
- Gehloff, M., M. Closen, and F. Lam. *Reduced edge distances in bolted timber moment connections with perpendicular to grain reinforcements*. in *World Conference on Timber Engineering*. 2010.
- Lam, F., et al. *Moment resistance of bolted timber connections with perpendicular to grain reinforcements*. in *Proceedings of the 10th World Conference on Timber Engineering (WCTE)*. 2008.
- Dong, W., et al., *Experimental Testing and Analytical Modeling of Glulam Moment Connections with Self-Drilling Dowels*. *Journal of Structural Engineering*, 2021. **147**(5).
- Australian Building Codes Board, *National Construction Code 2019*. 2019.
- Hansson, M. and H.J. Larsen, *Recent failures in glulam structures and their causes*. *Engineering Failure Analysis*, 2005. **12**(5): p. 808-818.
- Frühwald, E., et al., *Design of Safe Timber Structures - How Can we Learn from Structural Failures in Concrete, Steel and Timber?* 2007.
- Gilbert, B.P., et al., *Shear performance of glued and screwed timber-steel composite connections for composite timber-steel beams*. *Construction and Building Materials*, 2024. **450**.
- Núñez-Decap, M., et al., *Use of Carbon and Basalt Fibers with Adhesives to Improve Physical and Mechanical Properties of Laminated Veneer Lumber*. *Applied Sciences*, 2023. **13**(18): p. 10032.
- Wdowiak-Postulak, A., et al., *Load and Deformation Analysis in Experimental and Numerical Studies of Full-Size Wooden Beams Reinforced with Prestressed FRP and Steel Bars*. *Applied Sciences*, 2023. **13**(24): p. 13178.
- Alam, P., M.P. Ansell, and D. Smedley, *Mechanical repair of timber beams fractured in flexure using bonded-in reinforcements*. *Composites Part B: Engineering*, 2009. **40**(2): p. 95-106.
- De Luca, V. and C. Marano, *Prestressed glulam timbers reinforced with steel bars*. *Construction and Building Materials*, 2012. **30**: p. 206-217.
- Jasieńko, J. and T.P. Nowak, *Solid timber beams strengthened with steel plates – Experimental studies*. *Construction and Building Materials*, 2014. **63**: p. 81-88.
- Jurkiewicz, B., S. Durif, and A. Bouchair, *Behaviour of steel-timber beam in bending*. *ce/papers*, 2017. **1**(2-3): p. 2283-2291.
- Jurkiewicz, B., et al., *Experimental and analytical study of hybrid steel-timber beams in bending*. *Structures*, 2022. **39**: p. 1231-1248.
- Gharaibeh, L. and G. Doudak. *Structural performance of reinforced glulam beams*. in *World Conference on Timber Engineering (WCTE 2023)*. 2023. World Conference on Timber Engineering (WCTE 2023).
- Nabati, A., T. Ghanbari-Ghazijahani, and H.R. Valipour, *Innovative flitch sandwich beams with steel core under four-point bending*. *Engineering Structures*, 2021. **233**.
- Haase, P., et al., *Bending Behavior of Hybrid Timber-Steel Beams*. *Materials (Basel)*, 2024. **17**(5).
- Jansson, B., *Impact Loading of Timber Beams*, in *Faculty of Applied Science, Department of Civil Engineerin*. 1992, The University of British Columbia.
- Mindess, S. and B. Madsen, *The fracture of wood under impact loading*. *Materials and Structures*, 1986. **19**(1): p. 49-53.
- Wood, L.W., *Relation of strength of wood to duration of load*. 1960, U. S. Department of Agriculture.

22. Leijten, A.J.M., *Impact crash and simulation of timber beams*. 2001.
23. Baumann, G., et al., *A Comparative Study on the Temperature Effect of Solid Birch Wood and Solid Beech Wood under Impact Loading*. Materials (Basel), 2021. **14**(24).
24. Wight, N., C. Viau, and P. Heffernan, *Behaviour of glued-laminated timber beams under impact loading*. Canadian Journal of Civil Engineering, 2024. **51**(7): p. 753-768.
25. Cao, A.S., M. Houen, and A. Frangi, *Impact loading of glued laminated timber beams without finger-joints*. Computers & Structures, 2024. **296**.
26. Sukontasukkul, P., F. Lam, and S. Mindess, *Fracture of parallel strand lumber (PSL) under impact loading*. Materials and Structures, 2000. **33**(7): p. 445-449.
27. Doudak, G., C. Viau, and D.N. Lacroix, *Proposed Design Methods for Timber Members Subjected to Blast Loads*. Journal of Performance of Constructed Facilities, 2022. **36**(3).
28. Lacroix, D., et al., *Enhancing the performance of light-frame wood studs using glass fibre-reinforced polymers*. Engineering Structures, 2021. **245**.
29. Lacroix, D.N., C. Viau, and G. Doudak, *Flexural response of glued laminated (glulam) beams subjected to blast loads*, in *WCTE 2014*. 2014: Quebec city, Canada.
30. Oliveira, D., C. Viau, and G. Doudak, *Behaviour of mass timber members subjected to consecutive blast loads*. International Journal of Impact Engineering, 2023. **173**.
31. Poulin, M., et al., *Experimental and Analytical Investigation of Cross-Laminated Timber Panels Subjected to Out-of-Plane Blast Loads*. Journal of Structural Engineering, 2018. **144**(2).
32. Muñoz, W., et al., *Determination of yield point and ductility of timber assemblies: in search for a harmonised approach*. Engineered Wood Products Association, 2008. **41**.
33. ASTM International, *Standard Test Methods for Evaluating Properties of Wood-Base Fiber and Particle Panel Materials*. 2020, American Society for Testing and Materials: West Conshohocken, PA.
34. Taheri, A., A.S. Moghadam, and A.A. Tasnimi, *Critical factors in displacement ductility assessment of high-strength concrete columns*. International Journal of Advanced Structural Engineering, 2017. **9**(4): p. 325-340.
35. Park, R., *Evaluation of ductility of structures and structural assemblages from laboratory testing*. Bulletin of the New Zealand Society for Earthquake Engineering, 1989. **22**(3): p. 155-166.
36. Gao, W.-Y., T.-C. Wang, and K.-X. Hu, *Chapter 9 - Flexural behavior of fire-damaged RC slabs strengthened with basalt fabric-reinforced engineered cementitious composite (ECC)*, in *Advances in Engineered Cementitious Composites*, Y.X. Zhang and K. Yu, Editors. 2022, Woodhead Publishing. p. 287-318.
37. Bakalarz, M.M. and P.G. Kossakowski, *Ductility and Stiffness of Laminated Veneer Lumber Beams Strengthened with Fibrous Composites*. Fibers, 2022. **10**(2).
38. Mindess, S., P. Sukontasukkul, and F. Lam, *Fracture of air-dried and fully saturated parallel strand lumber (PSL) under impact loading*. Wood Science and Technology, 2004. **38**(3): p. 227-235.
39. Banthia, N., et al., *Impact testing of concrete using a drop-weight impact machine*. Experimental Mechanics, 1989. **29**(1): p. 63-69.
40. Bakhshi, M., et al., *Experimental and Analytical Study of the High-Strain Rate Flexural Behavior of SFRC*. Journal of Materials in Civil Engineering, 2024. **36**(4).